

UC Berkeley

UC Berkeley Previously Published Works

Title

Quantifying Species Populations in Multivalent Borohydride Electrolytes

Permalink

<https://escholarship.org/uc/item/62n0306z>

Journal

The Journal of Physical Chemistry B, 125(14)

ISSN

1520-6106

Authors

Hahn, Nathan T
Self, Julian
Han, Kee Sung
[et al.](#)

Publication Date

2021-04-15

DOI

10.1021/acs.jpcc.1c00263

Peer reviewed

Quantifying Species Populations in Multivalent Borohydride Electrolytes

Nathan T. Hahn,^{a,b,*} Julian Self,^{a,c,d} Kee Sung Han,^{a,e} Vijayakumar Murugesan,^{a,e} Karl T. Mueller,^{a,e} Kristin A. Persson,^{a,c,f} Kevin R. Zavadil^{a,b}

^aJoint Center for Energy Storage Research, Lemont, IL, 60439

^bMaterial, Physical and Chemical Sciences Center, Sandia National Laboratories, Albuquerque, NM 87185

^cDepartment of Materials Science and Engineering, University of California, Berkeley, CA 94720

^dEnergy Technologies Area, Lawrence Berkeley National Laboratory, Berkeley, CA 94720

^ePhysical and Computational Sciences Directorate, Pacific Northwest National Laboratory, Richland, WA 99354

^fThe Molecular Foundry, Lawrence Berkeley National Laboratory, Berkeley, CA 94720

Abstract

Multivalent batteries represent an important beyond Li-ion energy storage concept. The prospect of calcium batteries in particular has emerged recently due to novel electrolyte demonstrations, especially that of a ground-breaking combination of the borohydride salt $\text{Ca}(\text{BH}_4)_2$ dissolved in tetrahydrofuran. Recent analysis of magnesium and calcium versions of this electrolyte led to the identification of divergent speciation pathways for Mg^{2+} and Ca^{2+} despite identical anions and solvents, owing to differences in cation size and attendant flexibility of coordination. To test these proposed speciation equilibria and develop a more quantitative understanding thereof, we have applied pulsed-field-gradient nuclear magnetic resonance and dielectric relaxation spectroscopy to the study of these electrolytes. Concentration-dependent variation in anion diffusivities and solution dipole relaxations, interpreted with the aid of molecular dynamics simulations, confirm these divergent Mg^{2+} and Ca^{2+} speciation pathways. These results provide a more quantitative description of the electroactive species populations. We find that these species are present in relatively small quantities, even in the highly active $\text{Ca}(\text{BH}_4)_2$ /tetrahydrofuran electrolyte. This finding helps interpret previous characterizations of metal deposition efficiency and morphology control and thus provides important fundamental insight into the dynamic properties of multivalent electrolytes for next generation batteries.

Key Words: magnesium battery, calcium battery, spectroscopy, electrochemistry, energy storage

Introduction

Li-ion batteries have come to dominate the global portable electronics and electrified vehicle markets, but further advances in batteries are required to meet anticipated energy storage needs for a diversity of applications.¹ Among the proposed avenues toward this goal, multivalent batteries, including Ca, Mg, Zn, and Al, are intriguing options due to the high energy densities and generally lower reactivities of their metallic anodes compared to Li.² The alkaline earth chemistries of Mg and Ca have received growing interest recently due to their significantly negative redox potentials, yielding the prospect of high cell voltage.²⁻⁴ These high voltages, however, come at the cost of electrolyte stability, which must be managed to maintain high efficiencies and rates for the corresponding metal plating and stripping reactions. Because of this requirement, early stage electrolyte demonstrations have largely originated from exotic formulations containing reducing salts including organometallics facilitated by chloride dissolved in ethereal solvents such as tetrahydrofuran (THF).⁵⁻⁶ One of the first non-halide magnesium salts demonstrated to reversibly deposit Mg was $\text{Mg}(\text{BH}_4)_2$,⁷⁻⁸ and the first such calcium salt to function in this manner at room temperature was $\text{Ca}(\text{BH}_4)_2$.⁹ The ground-breaking nature of these electrolytes highlights the importance of the borohydride class as a system of fundamental study, despite its obvious drawbacks from the standpoint of oxidative reactivity. Moreover, understanding the links between borohydride solvation environments and properties has high potential impact for both solid-state electrolytes and reversible hydrogen storage, areas in which borohydrides are under active investigation.¹⁰⁻¹³

While several investigations into the liquid solvation environment of $\text{Mg}(\text{BH}_4)_2$ electrolytes have been conducted,^{7-8, 14-17} understanding of $\text{Ca}(\text{BH}_4)_2$ electrolyte solvation is relatively nascent.¹⁸⁻¹⁹ Our recent findings underscored the importance of BH_4^- coordination in determining speciation and delivery of the metal cation to the interface.¹⁹ The most probable ionic species determined from density-functional theory (DFT) calculations were found to be CaBH_4^+ and $\text{Ca}(\text{BH}_4)_3^-$, indicating that the electroactive species is the cationic cluster CaBH_4^+ . Difficulty in forming the active species, whether in $\text{Ca}(\text{BH}_4)_2/\text{THF}$ at low salt

concentrations (≤ 0.5 M) or in $\text{Mg}(\text{BH}_4)_2/\text{THF}$ across all salt concentrations, reduces the measured metal deposition current density and Coulombic efficiency.¹⁹ These findings also implicated the role of multimer formation in facilitating the creation of these important ionic species based on X-ray absorption spectroscopy; a key feature differentiating the behavior of the Mg and Ca electrolytes based on their configurational flexibility differences. The term “configurational flexibility” reflects the fact that Ca^{2+} can adopt a wider range of bonding configurations due to its greater size and polarizability than Mg^{2+} .²⁰⁻²¹ In order to validate these proposed speciation details from a more quantitative perspective, we report complimentary investigation into $\text{Mg}(\text{BH}_4)_2$ and $\text{Ca}(\text{BH}_4)_2$ solutions in THF *via* pulsed-field-gradient nuclear magnetic resonance (PFG-NMR) and dielectric relaxation spectroscopy (DRS). The results of this investigation confirm a significantly greater population of electroactive ionic species in the Ca system, which is particularly enhanced at high salt concentrations. By using molecular dynamics (MD) simulations to interpret the DRS data we are able to provide a quantitative estimation of the primary species in solution. We demonstrate the dominance of neutral monomers in $\text{Mg}(\text{BH}_4)_2/\text{THF}$ across the full concentration range and the enhancement of neutral dimers and ionic species in $\text{Ca}(\text{BH}_4)_2/\text{THF}$ at high salt concentrations. Despite the enhancement of electroactive CaBH_4^+ at high concentrations in the Ca case, the relative population of this species is still only a small fraction of the total Ca^{2+} inventory. This fact has important ramifications for sustaining high rate and energy efficient calcium plating from this electrolyte.

Methods

Electrolyte Preparation: Electrolyte synthesis was performed inside a catalyst-purified, argon filled glove box (MBraun) with typical water and oxygen levels below 1 ppm and 0.1 ppm, respectively. THF was purchased from Sigma-Aldrich, distilled over sodium, and stored over activated alumina and 3A molecular sieves prior to use, yielding measured water levels below 10 ppm. $\text{Ca}(\text{BH}_4)_2 \cdot 2\text{THF}$, $\text{Mg}(\text{BH}_4)_2$ (95%), and LiBH_4 (95%) salts were purchased from Sigma-Aldrich and used as received. Ionic conductivities were measured using electrochemical impedance spectroscopy in a custom cell consisting of parallel Pt electrodes, the cell constant of which was determined using aqueous KCl solutions.

PFM-NMR: D_{anion} and D_{solvent} were determined simultaneously by ^1H PFM-NMR using a bipolar gradient PFM sequence at 25 °C on a 600 MHz NMR spectrometer (Agilent, USA) equipped with a 5 mm z-gradient probe (Doty Scientific, USA). The PFM-echo profiles were obtained as a function of gradient strength (g) with a gradient length (δ) and a diffusion delay fixed at 2 and 30 ms, respectively. The gradient strength was gradually increased in 16 equal steps to the maximum applied gradient strength to observe the full decay in the echo profiles. The recorded echo profiles, $S(g)$ were fitted with the Stejskal-Tanner equation,²²

$$S(g) = S(0)\exp\left[-D(\gamma g\delta)^2\left(\Delta - \frac{\delta}{3}\right)\right] \quad (1)$$

where $S(0)$ is the echo intensity at gradient strength of zero. D , γ , δ , and Δ are the diffusion coefficient, the gyromagnetic ratio ($\gamma(^1\text{H}) = 2\pi \cdot 42.577 \text{ rad}\cdot\text{MHz}\cdot\text{T}^{-1}$), the gradient length, and the time interval between the two bipolar gradient pairs, respectively. ^{43}Ca and ^{25}Mg PFM-NMR were not successful for the determination of D_{cation} for Ca^{2+} and Mg^{2+} in these solutions due to the fast nuclear relaxation rates for ^{43}Ca and ^{25}Mg in these samples.

Dielectric Relaxation Spectroscopy: DRS was performed on electrolytes in glass vials using a dielectric probe kit (Keysight N1501A) and vector network analyzer (Keysight 9375A) over a frequency range of 0.5 to 26.5 GHz. Each set of measurements were performed with three-point calibration using air, a shorting block, and THF. Duplicate measurements were performed after recalibration to ensure consistency. Simultaneous fitting of the real (ε') and imaginary (ε'') components of the complex, frequency-dependent relative permittivity (eq. 2) was performed numerically by deconvolution of the individual dipole relaxation processes (eq. 3).²³

$$\varepsilon(\nu) = \varepsilon'(\nu) - i\varepsilon''(\nu) \quad (2)$$

$$\varepsilon(\nu) = \varepsilon_{\infty} + \sum_{j=1}^n \varepsilon_j \left[1 - (i2\pi\nu\tau_j)^{1-\alpha_j}\right]^{-1} \quad (3)$$

In eq. 3, ϵ_∞ accounts for the total intramolecular polarizability of the solution while the n solution dipole re-orientation contributions are included in the summation term based on each dipole's permittivity amplitude (ϵ), relaxation time (τ), and broadening or Cole-Cole parameter (α). For Debye relaxations $\alpha = 0$. Ionic conductivities (used to extract ϵ'' from the permittivity data) measured by impedance spectroscopy were treated as fixed parameters during the fitting process. It was determined that spectra obtained from the $\text{Mg}(\text{BH}_4)_2/\text{THF}$ solutions were best fit by one Debye relaxation for the solvent and one Cole-Cole relaxation for the salt while spectra from $\text{Ca}(\text{BH}_4)_2/\text{THF}$ solutions were best fit by two to three Debye relaxations. Summation of these relaxation amplitudes yields the total dielectric constant, ϵ_r , of the solution (see supporting information for fitting parameters, Table S1 and S2). The 1.0 M $\text{Mg}(\text{BH}_4)_2$ solution was observed to react at the probe tip, nucleating small bubbles which impacted the measured parameters. The data reported for this system were thus averaged over completely independent electrolyte makeups and calibrations (see supporting information, Table S2). The conclusions are not impacted by the uncertainty in this datapoint. Aside from the 1.0 M $\text{Mg}(\text{BH}_4)_2$ solution, the samples showed consistent dielectric constants in repeated measurements (typically better than ± 0.05). Species populations were determined by combining the measured dielectric constant changes with calculated dielectric increments ($\Delta\epsilon$) and $A/A_{\text{NMR,eff}}$ measurements, as described in the supporting information document.

Computational Simulations: Dielectric increment calculations were done with classical molecular dynamics simulations, as discussed in previous publications.²⁴⁻²⁵ Single salt species (such as CIPs, etc.) were placed in a box with 112 THF solvent molecules (approx. 0.10-0.11 M) using PACKMOL. With the GROMACS MD software, these electrolytes were equilibrated first using a Berendsen barostat (NPT), followed by heating and cooling steps. Afterwards, production runs in the NVT ensemble using the velocity rescaling thermostat were undertaken. In these regimes, salt species were associated for the duration of the simulation (each at least 10 ns) and from their dipole moment, in addition to the dipole moment of the solvent species, the dielectric constant of the entire electrolyte solution was found. The dielectric constant of the neat THF solution was subtracted from this value, which was then subsequently divided by the concentration (e.g.

0.11 M) to obtain the dielectric increment per salt species, as appearing in the supporting information (Table S3, Table S4 and Figure S4). For associated salt species with an overall charge, the overall charge was subtracted from the dipole moment as discussed in a previous publication.²⁴ The forcefield parameter files for BH_4^- were the same as those from Rajput et al.,^{19,26} the THF force field files from Caleman et al. and the Ca and Mg forcefield files from the standard OPLS forcefield.²⁷⁻²⁸ Error estimates appearing in Table S3 and S4 were calculated from duplicate simulations and analyses.

Results and Discussion

An increase in relative electroactive ionic species populations with overall salt concentration is demonstrated in that the ionic conductivities of both $\text{Mg}(\text{BH}_4)_2/\text{THF}$ and $\text{Ca}(\text{BH}_4)_2/\text{THF}$ solutions increase with concentration despite a drop in average BH_4^- diffusivity. Although the conductivity increase is much more dramatic for $\text{Ca}(\text{BH}_4)_2$ than for $\text{Mg}(\text{BH}_4)_2$, both increase significantly on a relative basis (Figure 1a). When the conductivity values are normalized by concentration yielding molar conductivities, Λ , the positive trends persist up to 1 M (supporting information, Figure S1). An increase in Λ should represent an increase either in the ionicity (relative formation of ionic species) of the electrolyte or in the diffusivities of the ionic species. Since the PFG-NMR measured diffusivity of BH_4^- (D_{anion}) decreases by nearly a factor of two in both solutions as concentration increases from 0.1 to 1.0 M (Figure 1b), the dominant factor must be an ionicity increase. This increase is clearly enhanced in the Ca system.

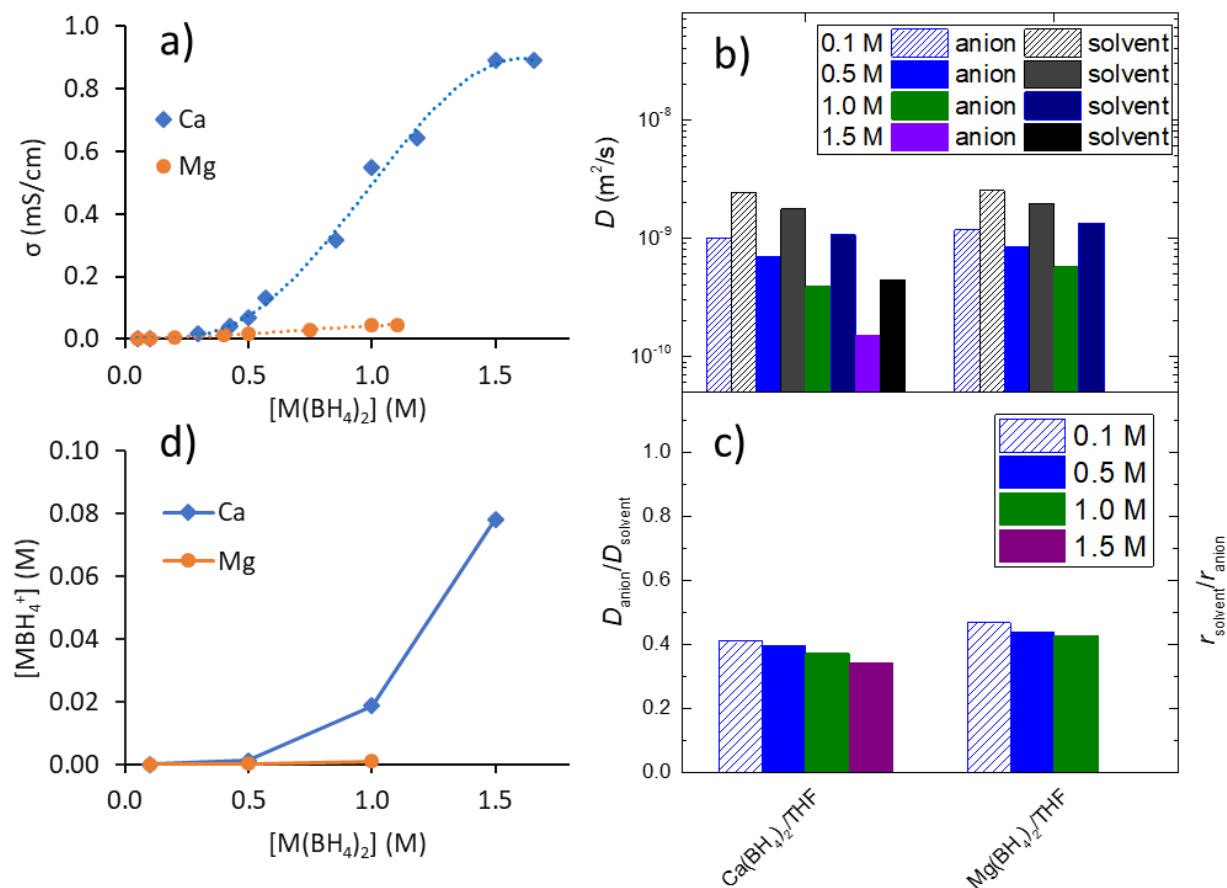
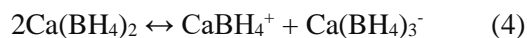


Figure 1. a) Ionic conductivity values measured for Mg(BH₄)₂ and Ca(BH₄)₂ in THF as a function of concentration (reproduced in part from Ref. 19 with permission from the Royal Society of Chemistry). Dotted lines represent polynomial fits serving as guides to the eye. b) Diffusivity values of BH₄⁻ and THF measured by PFG-NMR as a function of borohydride salt concentration. c) The relative diffusivities of anion to solvent calculated from the PFG-NMR data. d) Calculated concentrations of CaBH₄⁺ and MgBH₄⁺ in solution as a function of overall salt concentration based on an effective ionicity ratio analysis, assuming ionic species of MBH₄⁺ and M(BH₄)₃⁻.

The significant ionicity increase in these solutions occurs despite their strong ion pairing tendencies. The presence of extensive ion pairing is demonstrated by the relative anion and solvent diffusivities as measured by PFG-NMR. As shown in Figure 1b, the decrease in D_{anion} is accompanied by a decrease in THF diffusivity (D_{solvent}) with increasing concentration. This can be attributed to both an increase in solution viscosity (η) and an increased fraction of THF bound to the metal cations. To account for the solution viscosity changes, the ratio of $D_{\text{anion}}/D_{\text{solvent}}$ was calculated in each case (Figure 1c). Viscosity should affect both anion and solvent diffusivities in a similar manner based on the Stokes-Einstein

relation $D \sim (\eta R)^{-1}$, where R is the effective radius of the solution species. In all solutions D_{anion} is less than half of D_{solvent} , despite that fact that the calculated radius of gyration (R_g) of BH_4^- from MD simulations ($R_g = 0.6 \text{ \AA}$) is smaller than that of THF ($R_g = 1.4 \text{ \AA}$). This difference in R_g means that a “free” BH_4^- anion should diffuse much faster than a free THF molecule. The fact that $D_{\text{anion}} < D_{\text{solvent}}$ indicates that most, if not all, of the BH_4^- anions are coordinated to metal cations, forming clusters with significantly larger effective radii than free BH_4^- and yielding a lower average D_{anion} value. Indeed, the calculated R_g values for associated clusters from MD simulations are between 2.5 and 4.5 \AA , i.e. approximately twice as large as the R_g of THF. This size difference is generally consistent with the measured $D_{\text{anion}}/D_{\text{solvent}}$ values (supporting information, Tables S3 and S4).

The absence of free BH_4^- is consistent with previously reported Raman measurements that were unable to detect free BH_4^- in these electrolytes and with DFT calculations showing that dissociation of BH_4^- from Ca^{2+} or Mg^{2+} is unfavorable.^{15, 19} Indeed, even the dissociation of BH_4^- from Li^+ is highly unfavorable in THF.²⁹ Furthermore, DFT calculations indicated that the primary ionic species in $\text{Ca}(\text{BH}_4)_2/\text{THF}$ are most likely the associated clusters CaBH_4^+ and $\text{Ca}(\text{BH}_4)_3^-$, in which case the overall equilibrium could be considered as,



The differences in measured λ between the Ca^{2+} and Mg^{2+} electrolytes imply that these clusters form much more readily from $\text{Ca}(\text{BH}_4)_2$ than from $\text{Mg}(\text{BH}_4)_2$ in THF. The fact that $D_{\text{anion}}/D_{\text{solvent}}$ decreases with increasing concentration in both $\text{Ca}(\text{BH}_4)_2$ and $\text{Mg}(\text{BH}_4)_2$ solutions confirms that enhanced populations of free BH_4^- (which would increase $D_{\text{anion}}/D_{\text{solvent}}$) are not the origin of the ionicity increases. If anything, this trend implies that some degree of salt aggregation is favored at high concentrations in both solutions, although previous work indicated that $\text{Ca}(\text{BH}_4)_2$ more readily forms multimeric species than $\text{Mg}(\text{BH}_4)_2$ in THF.^{19, 30-33} These results validate our hypothesis that the primary origin of the increasing λ vs. concentration trend in alkaline earth borohydride solutions is the enhanced formation of associated ionic clusters such as MBH_4^+ rather than liberation of free BH_4^- or a possible increase in ion diffusivity.³⁴

Considering these results in light of the proposed ionic species (MBH_4^+ and $\text{M}(\text{BH}_4)_3^-$),¹⁹ we estimate their concentrations from the measured Λ and D_{anion} values based on an effective ionicity ratio $\Lambda/\Lambda_{\text{NMR,eff}}$ (i.e. effective Haven ratio), where $\Lambda_{\text{NMR,eff}}$ is the molar conductivity expected if all the dissolved salt is converted into the proposed ionic species. This value is given by eq. 5,³⁵

$$\Lambda_{\text{NMR,eff}} = \frac{eF}{k_B T} \left(\frac{D_i z_i c_i}{c_{\text{salt}}} + \frac{D_j z_j c_j}{c_{\text{salt}}} \right) \quad (5)$$

In eq. 5, species i and j refer to MBH_4^+ and $\text{M}(\text{BH}_4)_3^-$, respectively, D is the species self-diffusion coefficient, z is the species charge, c is the species concentration, and c_{salt} is the overall salt concentration. Therefore, $z_i = z_j = 1$, and $c_i/c_{\text{salt}} = c_j/c_{\text{salt}} = 0.5$ based on stoichiometry. To a first approximation it is assumed that $D_i = D_j$, i.e. $D(\text{MBH}_4^+) = D(\text{M}(\text{BH}_4)_3^-)$, and that these diffusivities are approximately equal to the ensemble measured anion (BH_4^-) diffusivity. These assumptions are based on the lack of free BH_4^- and on the similarity of the calculated R_g values for the resulting metal-borohydride clusters in MD simulations (supporting information, Tables S3 and S4). Furthermore, the charged cluster diffusivities are not expected to differ much from those of the neutral clusters.³⁶⁻³⁷ The contributions of the charged clusters to $\Lambda_{\text{NMR,eff}}$ are approximated as ideal, i.e. long-range interionic interactions are neglected. Thus, ionic populations estimated from the effective ionicity may be somewhat underestimated. The MBH_4^+ concentrations resulting from this analysis are shown in Figure 1d. These calculations highlight the remarkable increase in concentration of these electroactive species as a function of overall salt concentration in the Ca system. These species are almost non-existent at salt concentrations less than 0.5 M, which readily explains the severely inhibited calcium electrodeposition response reported at such concentrations.¹⁹ Since the Mg system possesses very low concentrations of MgBH_4^+ at all salt concentrations, its metal deposition response is inhibited even at high salt concentrations. This is consistent with previous reports demonstrating that alkali-salt additives (LiBH_4 or NaBH_4) are required to achieve adequate magnesium electrodeposition rate and reversibility.^{7, 15-16, 38}

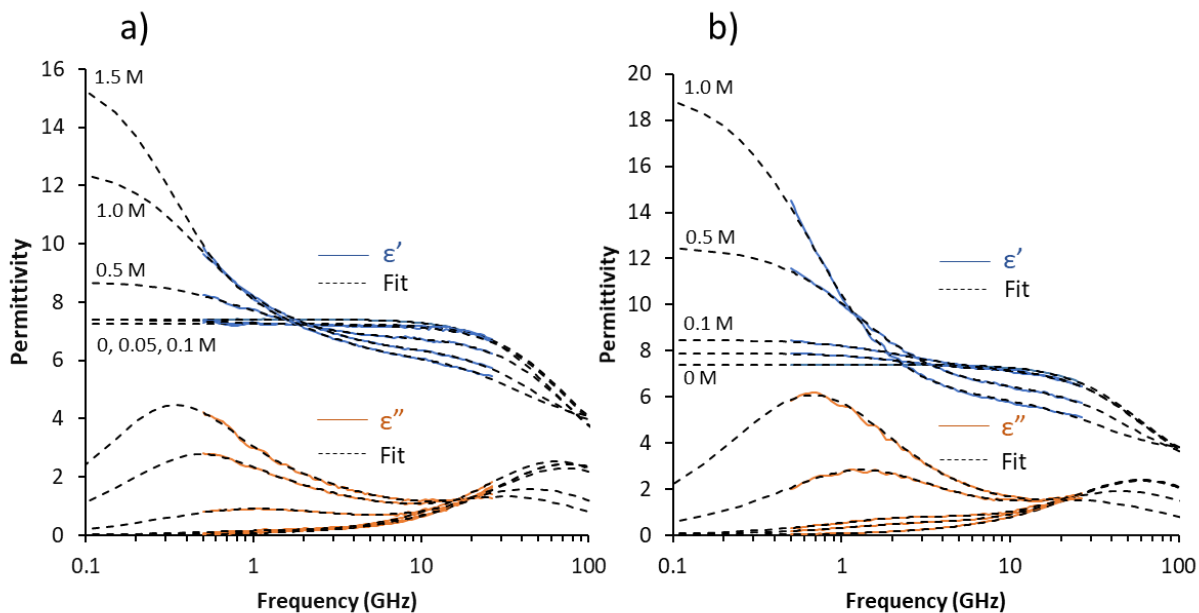


Figure 2. Real (ϵ' , top) and imaginary (ϵ'' , bottom) components of the complex permittivity measured as a function of frequency in a) $\text{Ca}(\text{BH}_4)_2/\text{THF}$ and b) $\text{Mg}(\text{BH}_4)_2/\text{THF}$. Solid lines represent the measured data while dashed lines represent fits of the data based on a summation of Debye and/or Cole-Cole relaxations. Deconvolutions of these relaxations are shown in the supporting information, Figure S2.

Significant differences in the concentration-dependent speciation pathways of the Mg and Ca electrolytes are manifested in the complex permittivity responses of the solvated species. DRS spectra measured across a range of salt concentrations in these two systems reveal their characteristic frequency-dependent permittivity (Figure 2). In both systems two primary relaxations are observed: a high frequency solvent relaxation ($f \sim 30$ to 70 GHz), and a low frequency relaxation corresponding to dipolar salt clusters ($f \sim 0.3$ to 3 GHz). The relaxation frequencies of the $\text{Ca}(\text{BH}_4)_2$ salt clusters are somewhat lower than those of $\text{Mg}(\text{BH}_4)_2$, presumably due to the larger size of Ca^{2+} and its related complexes. In $\text{Ca}(\text{BH}_4)_2/\text{THF}$ the impact of dipolar salt clusters on the solution permittivity is not significant until salt concentration exceeds 0.1 M while in $\text{Mg}(\text{BH}_4)_2/\text{THF}$ these clusters are significant even at 0.05 M. Due to the presence of these clusters, the dielectric constants (ϵ_r) of the concentrated solutions are far greater than that of the neat THF solvent ($\epsilon_r = 7.4$), reaching values as high as 18.2 for $\text{Mg}(\text{BH}_4)_2$ and 16.0 for $\text{Ca}(\text{BH}_4)_2$ (Figure 3a). Our observation of a net increase in ϵ_r is consistent with previous investigations of strongly associating alkali salts in low permittivity solvents.^{24, 39-41} Recently we speculated that ϵ_r could increase to a value as high as 10 in

Ca(BH₄)₂/THF due to such effects,¹⁹ but this value turns out to have been a significant underestimation. The most important difference in the permittivity behavior of the Mg and Ca systems lies in the functional forms of the ϵ_r vs. concentration dependence (Figure 3a). In Mg(BH₄)₂/THF, ϵ_r increases linearly across the entire concentration range while in Ca(BH₄)₂/THF the ϵ_r change is non-linear and even non-monotonic. The linear Mg(BH₄)₂ behavior implies an essentially static speciation profile in which one or more dipolar clusters are present at a constant relative population regardless of salt concentration. In contrast, the Ca(BH₄)₂ behavior implies an evolving speciation profile where the relative dipolar cluster populations vary significantly with salt concentration. This result speaks to the configurational flexibility differences of Ca²⁺ and Mg²⁺.¹⁹⁻²¹

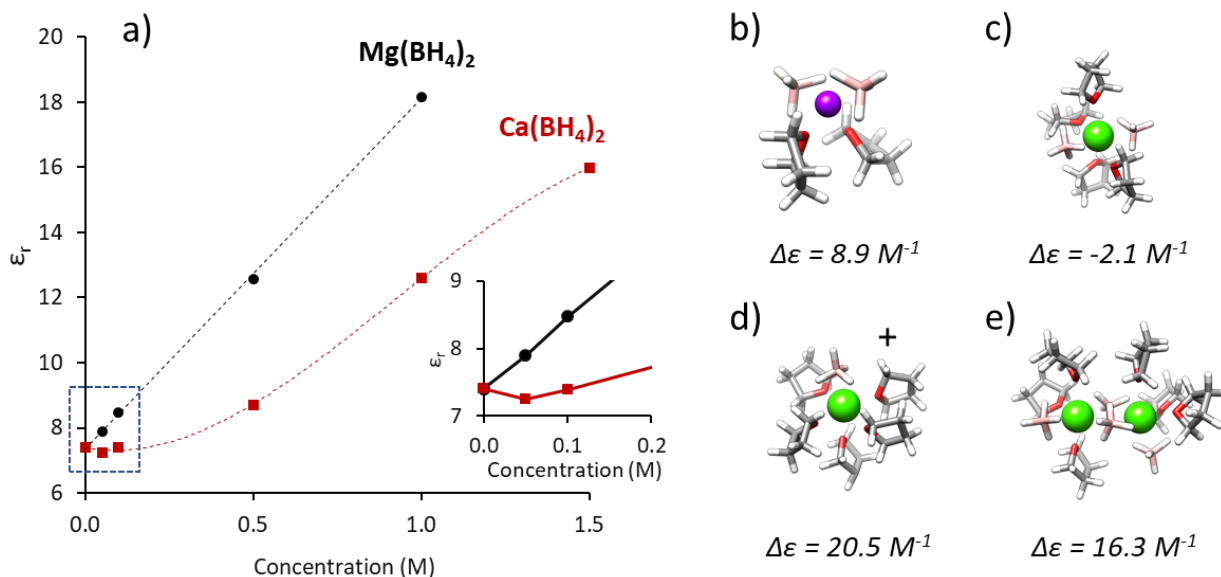


Figure 3. a) Solution dielectric constants (ϵ_r) determined from fits of the complex permittivity data as a function of concentration. Dotted lines represent trend lines for the ϵ_r vs. concentration data (linear in the case of Mg²⁺ and polynomial in the case of Ca²⁺). Inset: magnification of the plots at low concentrations. b-e) Representative cluster structures to which the ϵ_r changes are attributed. The calculated net dielectric increment ($\Delta\epsilon$) of each cluster is indicated. These species are referred to as: b) Mg neutral monomer, c) Ca neutral monomer, d) Ca CIP (contact-ion pair) cation, e) Ca neutral dimer (bent configuration). Mg, Ca, B, C, H and O atoms are shown in purple, green, pink, grey, white and red respectively. The calculated parameters and uncertainties of all species investigated are shown in Tables S3 and S4 in the supporting information.

Our previous investigations led us to conclude that the primary solvated species in Mg(BH₄)₂/THF is the neutral, monomeric form of the dissolved salt across all concentrations, based on the low measured

conductivities and the reported tendency of $\text{Mg}(\text{BH}_4)_2$ toward forming monomeric solvates.^{19, 31-32} To test whether such species could explain the linear and steeply sloped ϵ_r vs. concentration trend, the dielectric increments ($\Delta\epsilon$) of several clusters were simulated by MD; the parameter $\Delta\epsilon$ represents the net change in ϵ_r that a given cluster would induce when formed in a THF medium at a concentration of 1 M. The neutral monomer, $\text{Mg}(\text{BH}_4)_2$, possesses a highly asymmetric structure and a large dipole moment leading to a large computed net $\Delta\epsilon$ of 8.9 M^{-1} . This value agrees well with the net $\Delta\epsilon$ of 9.4 M^{-1} measured for this electrolyte across the entire concentration range (supporting information, Figure S3). This agreement suggests that these neutral monomers are the majority solvated species across this concentration range. We note that the small populations of MgBH_4^+ species predicted from conductivity and diffusivity analyses are unlikely to be observed by DRS due to their low concentration. For comparison, measurements of LiBH_4/THF as a simpler 1:1 salt system ostensibly dominated by neutral contact ion pairs (CIPs) in THF ($K_A \sim 10^9$)²⁹ also yielded a linear ϵ_r vs. concentration trend (supporting information, Figure S4). As in the Mg case, the $\Delta\epsilon$ derived from the LiBH_4 measurements agrees with the calculated $\Delta\epsilon$ value (9.2 vs. 9.7). This agreement between measured overall $\Delta\epsilon$ and calculated neutral monomer $\Delta\epsilon$ in both systems provides strong evidence that both systems are dominated by these species at the concentrations investigated. In previous studies, salt clusters composed of a single cation and two anions (“triple ions”) were sometimes presumed as linear and thus not detectable as dipolar species by DRS.^{40, 42} However, a more rigorous evaluation of cluster dielectric increments by MD simulations clearly shows that such structural assumptions can be misleading, as exemplified by the case of $\text{Mg}(\text{BH}_4)_2/\text{THF}$.

In $\text{Ca}(\text{BH}_4)_2/\text{THF}$ we recently proposed that neutral monomers ($\text{Ca}(\text{BH}_4)_2$) are prevalent at low salt concentrations and that these are progressively converted to multimeric and ionic species such as $\text{Ca}_2(\text{BH}_4)_4$, CaBH_4^+ , and $\text{Ca}(\text{BH}_4)_3^-$ as salt concentration is increased.¹⁹ Calculations of these species’ $\Delta\epsilon$ values indicates that our hypothesized trajectory of species evolution can explain the unique ϵ_r vs. concentration trend measured in this system (Figure 3). MD simulations reveal that the neutral calcium monomer is much more symmetric than the magnesium analog and has almost no dipole moment (Figure 3c), resulting in a $\Delta\epsilon$ of -2.1 M^{-1} . The negative $\Delta\epsilon$ arises from the fact that several THF molecules are bound to this solvated

cluster and can no longer contribute to the background dielectric constant. Therefore, a population of solvated neutral monomers can readily explain the small initial decrease in measured dielectric constant of ~ 0.1 units at 0.05 M (Figure 3a, inset). At concentrations above 0.1 M the measured dielectric constant increases significantly above that of neat THF, signaling a shift in the solution equilibria toward more polar clusters.

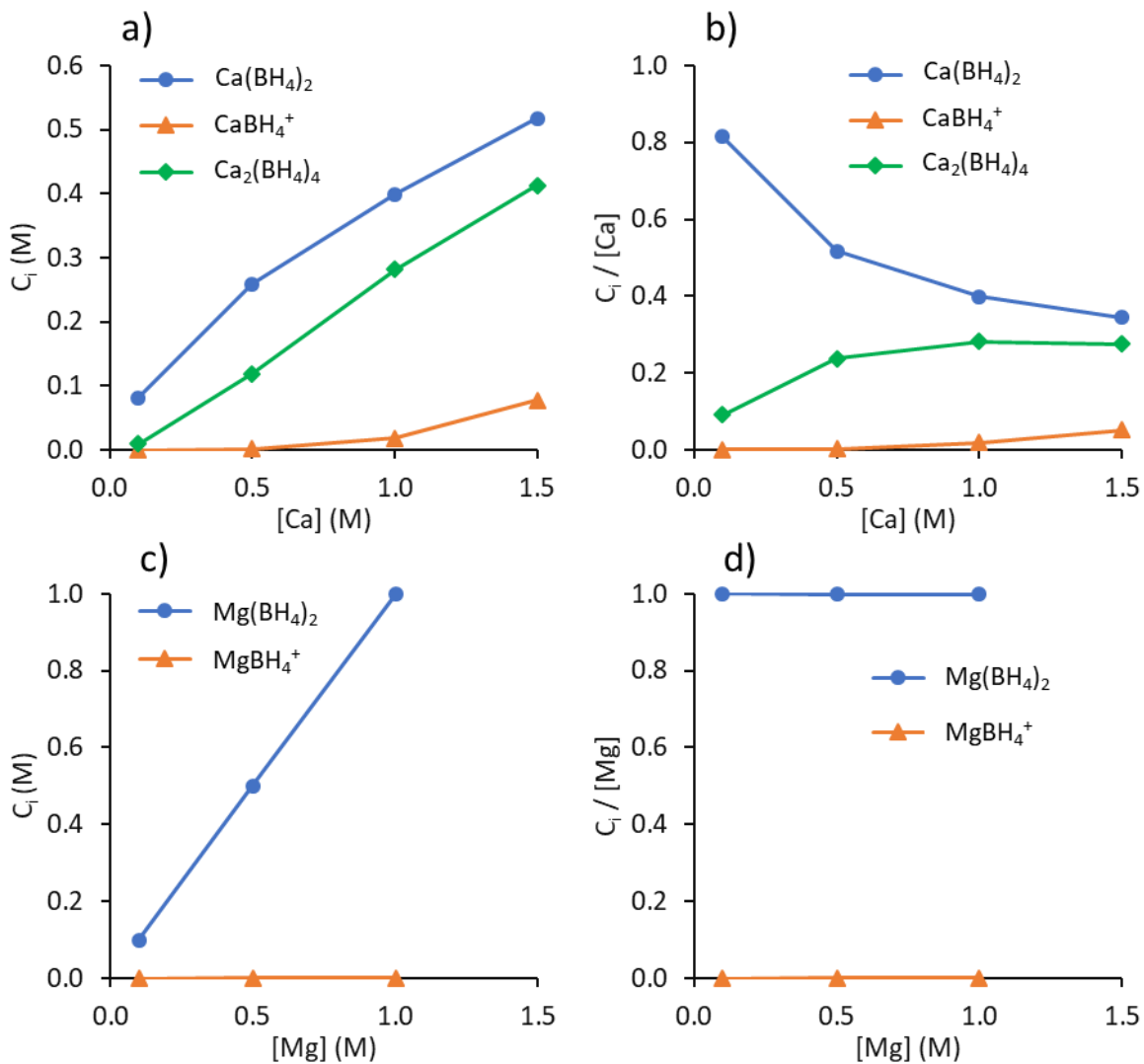
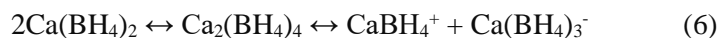


Figure 4. Concentrations of the major solvated species calculated from the effective ionicity analysis combined with DRS measurements and modeling as a function of overall salt concentration for a,b) $\text{Ca}(\text{BH}_4)_2/\text{THF}$ and c,d) $\text{Mg}(\text{BH}_4)_2/\text{THF}$. The data are plotted either a,c) as species concentrations or b,d) as relative populations. It is assumed that $[\text{MBH}_4^+] = [\text{M}(\text{BH}_4)_3^-]$.

Analysis of the hypothesized clusters reveals that both CaBH_4^+ ($\Delta\varepsilon = 20.5 \text{ M}^{-1}$) and $\text{Ca}_2(\text{BH}_4)_4$ ($\Delta\varepsilon = 16.3 \text{ M}^{-1}$) could contribute significantly to the permittivity increase measured in $\text{Ca}(\text{BH}_4)_2/\text{THF}$. The large dielectric increment of the dimer species is surprising given that neutral dimers are often assumed to have negligible dipole moments due to their approximately symmetric structure.^{40, 43} However, over our simulated MD trajectory we find that this $\text{Ca}_2(\text{BH}_4)_4$ cluster frequently rearranges into bent or pyramidal configurations, leading to a significant time-averaged dipole moment magnitude and a resulting dielectric increment of 16.3 M^{-1} (supporting information Figure S5). This again highlights the importance of MD simulations in accurately accounting for the range of conformations that a given cluster may adopt. The calculated $\Delta\varepsilon$ values allow for estimation of various species populations contributing to the overall measured $\Delta\varepsilon$ assuming an equilibrium distribution among the four proposed major species,



The MD-simulated $\Delta\varepsilon$ values of these species were used to calculate the self-consistent populations that could account for the measured overall $\Delta\varepsilon$ at each salt concentration. To bolster this approach, the calculations were refined by incorporating the CaBH_4^+ and $\text{Ca}(\text{BH}_4)_3^-$ concentrations predicted from the aforementioned effective ionicity analysis (as shown in Figure 1d). Without this input, the species populations cannot be inferred precisely due to difficulties in differentiating the contributions of CaBH_4^+ and $\text{Ca}_2(\text{BH}_4)_4$ to ε_r (supporting information, Figure S6). The calculated speciation diagrams (Figure 4a-b) reveal that the neutral monomer is the dominant species at low salt concentrations of 0.1 M and below, that these species are partially converted to dimers at moderate to high salt concentrations, and that small populations of the ionic species become stabilized at high salt concentrations. In $\text{Mg}(\text{BH}_4)_2/\text{THF}$, however, the neutral monomers are more strongly favored and almost no change in speciation is observed (Figure 4c-d).

The fact that dimers account for at least half of the total calcium inventory in $\text{Ca}(\text{BH}_4)_2/\text{THF}$ solutions at high salt concentrations ensures their detection *via* X-ray absorption spectroscopy,¹⁹ lending credence to these calculations. The high concentration of polar dimers and the resulting solution permittivity increase likely helps stabilize the ionic clusters. This phenomenon is analogous to the “re-dissociation”

mechanism proposed in previous investigations.^{24, 40, 44} However, this term usually refers to the facilitation of free ion formation, whereas in our case the increase in conductivity is caused by ionic cluster formation. To our knowledge, this is the first time that the stabilization of ionic clusters rather than free ions has been attributed to the accumulation of polar salt species. It is surprising that this stabilization mechanism does not operate as effectively in $\text{Mg}(\text{BH}_4)_2/\text{THF}$ despite its high concentration of polar monomers and larger relative increase in dielectric constant. We speculate that this is due to a smaller thermodynamic equilibrium constant for forming the necessary ionic clusters, i.e. MgBH_4^+ and $\text{Mg}(\text{BH}_4)_3^-$, due to the greater charge density and lesser polarizability of Mg^{2+} . Therefore, the configurational flexibility of Ca^{2+} remains an important criterion for effective ionic cluster formation in these strongly ion-associating solutions.

Although the proposed electroactive species CaBH_4^+ constitutes only a minority population in $\text{Ca}(\text{BH}_4)_2/\text{THF}$, the kinetics of species interconversion likely prevent CaBH_4^+ from becoming *selectively* depleted at the anode surface during calcium plating (i.e. cell charging). The kinetics of ion pairing and dissociation are generally fast enough, by many orders of magnitude,⁴⁵ to prevent species-specific depletion due to electrochemical consumption at an electrode, provided the overall concentration of salt is maintained. However, the concentration-dependent thermodynamics of speciation, as inferred from Figure 4, predict a strong suppression of $[\text{CaBH}_4^+]$ near the surface and in the diffusion layer if large salt concentration gradients are formed during high rate and/or high capacity calcium plating. This suppression of ionic species may lead to a significant Ohmic potential drop despite high bulk salt concentrations. Moreover, low concentrations of electroactive CaBH_4^+ near the electrode may promote parasitic reactions and loss of calcium morphology control. Indeed, a recent study highlighted that such rate-dependent calcium plating problems are encountered in $\text{Ca}(\text{BH}_4)_2/\text{THF}$ electrolytes.⁴⁶ Therefore, we propose the relatively small, concentration-dependent population of CaBH_4^+ as the underlying cause. Our findings thus inform both recent and ongoing efforts at studying interfacial phenomena in these unique electrolyte environments.

Conclusions

Complimentary analyses of ionic conductivity, anion diffusivity, and solution permittivity provide a quantitative understanding of solvation in an important class of alkaline earth metal borohydride electrolytes in THF. The primary findings of these analyses are: 1) both $\text{Mg}(\text{BH}_4)_2$ and $\text{Ca}(\text{BH}_4)_2$ electrolytes exhibit an increase in ionicity with concentration despite extensive ion pairing in both systems; 2) electroactive MBH_4^+ species populations are much more favored in the latter case, especially at high salt concentrations; 3) $\text{Mg}(\text{BH}_4)_2/\text{THF}$ is dominated by neutral monomers across the full concentration range while $\text{Ca}(\text{BH}_4)_2/\text{THF}$ speciation evolves from neutral monomers to multimers and ionic species; 4) the population of the electroactive CaBH_4^+ species in $\text{Ca}(\text{BH}_4)_2/\text{THF}$ is less than 0.1 M, even in high salt concentration electrolytes (1 to 1.5 M) that support high coulombic efficiency electrodeposition. The ability to quantify species populations in the $\text{Ca}(\text{BH}_4)_2/\text{THF}$ electrolyte represents an important contribution to the understanding of these systems that directly links to recent demonstrations of surface and interfacial phenomena.

Supporting Information. The following files are available free of charge. Ionic conductivity measurements, DRS methods, DRS fitting examples, DRS extracted parameters, cluster calculations, speciation diagrams.

Corresponding Author

*nthahn@sandia.gov

ACKNOWLEDGMENT

This work was supported by the Joint Center for Energy Storage Research, an Energy Innovation Hub funded by the U.S. Department of Energy. Sandia National Laboratories is a multimission laboratory managed and operated by National Technology & Engineering Solutions of Sandia, LLC, a wholly owned subsidiary of Honeywell International Inc., for the U.S. Department of Energy's National Nuclear Security Administration under contract DE-NA0003525. This research used resources of the National Energy Research Scientific Computing Center, a DOE Office of Science User Facility supported by the Office of

Science of the U.S. Department of Energy under contract no. DE-AC02-05CH11231. The PFG-NMR measurements were performed at the Environmental Molecular Sciences Laboratory (EMSL), a national scientific user facility sponsored by the DOE's Office of Biological and Environmental Research and located at Pacific Northwest National Laboratory (PNNL). This paper describes objective technical results and analysis. Any subjective views or opinions that might be expressed in the paper do not necessarily represent the views of the U.S. Department of Energy or the United States Government.

References

1. Trahey, L.; Brushett, F. R.; Balsara, N. P.; Ceder, G.; Cheng, L.; Chiang, Y.-M.; Hahn, N. T.; Ingram, B. J.; Minter, S. D.; Moore, J. S., et al., Energy storage emerging: A perspective from the joint center for energy storage research. *Proceedings of the National Academy of Sciences* **2020**, *117*, 12550.
2. Liang, Y.; Dong, H.; Aurbach, D.; Yao, Y., Current status and future directions of multivalent metal-ion batteries. *Nature Energy* **2020**, *5*, 646-656.
3. Ponrouch, A.; Frontera, C.; Bardé, F.; Palacín, M. R., Towards a calcium-based rechargeable battery. *Nature Materials* **2015**, *15*, 169.
4. Arroyo-de Dompablo, M. E.; Ponrouch, A.; Johansson, P.; Palacín, M. R., Achievements, challenges, and prospects of calcium batteries. *Chemical Reviews* **2019**.
5. Mizrahi, O.; Amir, N.; Pollak, E.; Chusid, O.; Marks, V.; Gottlieb, H.; Larush, L.; Zinigrad, E.; Aurbach, D., Electrolyte solutions with a wide electrochemical window for rechargeable magnesium batteries. *Journal of The Electrochemical Society* **2008**, *155*, A103-A109.
6. Viestfrid, Y.; Levi, M. D.; Gofer, Y.; Aurbach, D., Microelectrode studies of reversible mg deposition in thf solutions containing complexes of alkylaluminum chlorides and dialkylmagnesium. *Journal of Electroanalytical Chemistry* **2005**, *576*, 183-195.
7. Mohtadi, R.; Matsui, M.; Arthur, T. S.; Hwang, S.-J., Magnesium borohydride: From hydrogen storage to magnesium battery. *Angewandte Chemie International Edition* **2012**, *51*, 9780-9783.
8. Shao, Y.; Liu, T.; Li, G.; Gu, M.; Nie, Z.; Engelhard, M.; Xiao, J.; Lv, D.; Wang, C.; Zhang, J.-G., et al., Coordination chemistry in magnesium battery electrolytes: How ligands affect their performance. *Scientific Reports* **2013**, *3*, 3130.
9. Wang, D.; Gao, X.; Chen, Y.; Jin, L.; Kuss, C.; Bruce, P. G., Plating and stripping calcium in an organic electrolyte. *Nature Materials* **2017**, *17*, 16.
10. Lu, Z.; Ciucci, F., Metal borohydrides as electrolytes for solid-state Li, Na, Mg, and Ca batteries: A first-principles study. *Chemistry of Materials* **2017**, *29*, 9308-9319.
11. Cuan, J.; Zhou, Y.; Zhou, T.; Ling, S.; Rui, K.; Guo, Z.; Liu, H.; Yu, X., Borohydride-scaffolded Li/Na/Mg fast ionic conductors for promising solid-state electrolytes. *Advanced Materials* **2019**, *31*, 1803533.
12. He, T.; Cao, H.; Chen, P., Complex hydrides for energy storage, conversion, and utilization. *Advanced Materials* **2019**, *31*, 1902757.

13. Schneemann, A.; Wan, L. F.; Lipton, A. S.; Liu, Y.-S.; Snider, J. L.; Baker, A. A.; Sugar, J. D.; Spataru, C. D.; Guo, J.; Autrey, T. S., et al., Nanoconfinement of molecular magnesium borohydride captured in a bipyridine-functionalized metal–organic framework. *ACS Nano* **2020**, *14*, 10294-10304.
14. Samuel, D.; Steinhäuser, C.; Smith, J. G.; Kaufman, A.; Radin, M. D.; Naruse, J.; Hiramatsu, H.; Siegel, D. J., Ion pairing and diffusion in magnesium electrolytes based on magnesium borohydride. *ACS Applied Materials & Interfaces* **2017**, *9*, 43755-43766.
15. Deetz, J. D.; Cao, F.; Wang, Q.; Sun, H., Exploring the liquid structure and ion formation in magnesium borohydride electrolyte using density functional theory. *Journal of The Electrochemical Society* **2018**, *165*, A61-A70.
16. Deetz, J. D.; Cao, F.; Sun, H., Exploring the synergy of LiBH₄/NaBH₄ additives with mg(bh₄)₂ electrolyte using density functional theory. *Journal of The Electrochemical Society* **2018**, *165*, A2451-A2457.
17. Arthur, T. S.; Glans, P.-A.; Singh, N.; Tutusaus, O.; Nie, K.; Liu, Y.-S.; Mizuno, F.; Guo, J.; Alsem, D. H.; Salmon, N. J., et al., Interfacial insight from operando XAS/TEM for magnesium metal deposition with borohydride electrolytes. *Chemistry of Materials* **2017**, *29*, 7183-7188.
18. Ta, K.; Zhang, R. X.; Shin, M.; Rooney, R. T.; Neumann, E. K.; Gewirth, A. A., Understanding Caa electrodeposition and speciation processes in nonaqueous electrolytes for next-generation Caa-ion batteries. *ACS Applied Materials & Interfaces* **2019**, *11*, 21536-21542.
19. Hahn, N. T.; Self, J.; Seguin, T. J.; Driscoll, D. M.; Rodriguez, M. A.; Balasubramanian, M.; Persson, K. A.; Zavadil, K. R., The critical role of configurational flexibility in facilitating reversible reactive metal deposition from borohydride solutions. *Journal of Materials Chemistry A* **2020**, *8*, 7235-7244.
20. Katz, A. K.; Glusker, J. P.; Beebe, S. A.; Bock, C. W., Calcium ion coordination: A comparison with that of beryllium, magnesium, and zinc. *Journal of the American Chemical Society* **1996**, *118*, 5752-5763.
21. Carafoli, E.; Krebs, J., Why calcium? How calcium became the best communicator. *Journal of Biological Chemistry* **2016**.
22. Stejskal, E. O.; Tanner, J. E., Spin diffusion measurements: Spin echoes in the presence of a time-dependent field gradient. *The Journal of Chemical Physics* **1965**, *42*, 288-292.
23. Buchner, R.; Hefter, G., Interactions and dynamics in electrolyte solutions by dielectric spectroscopy. *Physical Chemistry Chemical Physics* **2009**, *11*, 8984-8999.
24. Self, J.; Hahn, N. T.; Fong, K. D.; McClary, S. A.; Zavadil, K. R.; Persson, K. A., Ion pairing and redissociation in low-permittivity electrolytes for multivalent battery applications. *The Journal of Physical Chemistry Letters* **2020**, *11*, 2046-2052.
25. Self, J.; Wood, B. M.; Rajput, N. N.; Persson, K. A., The interplay between salt association and the dielectric properties of low permittivity electrolytes: The case of LiPF₆ and LiAsF₆ in dimethyl carbonate. *The Journal of Physical Chemistry C* **2018**, *122*, 1990-1994.
26. Rajput, N. N.; Qu, X. H.; Sa, N.; Burrell, A. K.; Persson, K. A., The coupling between stability and ion pair formation in magnesium electrolytes from first-principles quantum mechanics and classical molecular dynamics. *Journal of the American Chemical Society* **2015**, *137*, 3411-3420.
27. Jorgensen, W. L.; Maxwell, D. S.; Tirado-Rives, J., Development and testing of the OPLS all-atom force field on conformational energetics and properties of organic liquids. *Journal of the American Chemical Society* **1996**, *118*, 11225-11236.

28. Caleman, C.; van Maaren, P. J.; Hong, M.; Hub, J. S.; Costa, L. T.; van der Spoel, D., Force field benchmark of organic liquids: Density, enthalpy of vaporization, heat capacities, surface tension, isothermal compressibility, volumetric expansion coefficient, and dielectric constant. *J. Chem. Theory Comput.* **2012**, *8*, 61-74.
29. Ashby, E. C.; Dobbs, F. R.; Hopkins, H. P., Composition of complex aluminum hydrides and borohydrides, as inferred from conductance, molecular association, and spectroscopic studies. *Journal of the American Chemical Society* **1973**, *95*, 2823-2829.
30. Bremer, M.; Nöth, H.; Thomann, M.; Schmidt, M., Preparation and molecular structures of tetrahydrofuran, diethylene diglycol dimethyl ether and 18-crown-6 complexes of strontium and barium tetrahydridoborate. *Chemische Berichte* **1995**, *128*, 455-460.
31. Bremer, M.; Nöth, H.; Warchhold, M., The structure of some amine solvates of magnesium bis(tetrahydroborate) and DFT calculations on solvates of lithium tetrahydroborate. *European Journal of Inorganic Chemistry* **2003**, *2003*, 111-119.
32. Lobkovskii, E. B.; Titov, L. V.; Psikha, S. B.; Antipin, M. Y.; Struchkov, Y. T., X-ray crystallographic investigation of crystals of bis(tetrahydroborato)tris(tetrahydrofuranato)magnesium. *Journal of Structural Chemistry* **1983**, *23*, 644-646.
33. Lobkovskii, E. B.; Chekhlov, A. N.; Levicheva, M. D.; Titov, L. V., Crystal and molecular structure of the complex of calcium borohydride with diethylene glycol diethyl ether. *Khoord. Khim.* **1988**, *14*, 543-550.
34. Petrowsky, M.; Frech, R.; Suarez, S. N.; Jayakody, J. R. P.; Greenbaum, S., Investigation of fundamental transport properties and thermodynamics in diglyme-salt solutions. *The Journal of Physical Chemistry B* **2006**, *110*, 23012-23021.
35. Takeuchi, M.; Kameda, Y.; Umebayashi, Y.; Ogawa, S.; Sonoda, T.; Ishiguro, S.-i.; Fujita, M.; Sano, M., Ion-ion interactions of LiPF₆ and LiBF₄ in propylene carbonate solutions. *J Mol Liq* **2009**, *148*, 99-108.
36. Cohen, L. H.; Saraf, D. N.; Witherspoon, P. A., Diffusion coefficients of hydrocarbons in water: Method for measuring. *Science* **1963**, *142*, 955.
37. Hall, J. R.; Wishaw, B. F.; Stokes, R. H., The diffusion coefficients of calcium chloride and ammonium chloride in concentrated aqueous solutions at 25°. *Journal of the American Chemical Society* **1953**, *75*, 1556-1560.
38. Chang, J.; Haasch, R. T.; Kim, J.; Spila, T.; Braun, P. V.; Gewirth, A. A.; Nuzzo, R. G., Synergetic role of Li⁺ during Mg electrodeposition/dissolution in borohydride diglyme electrolyte solution: Voltammetric stripping behaviors on a Pt microelectrode indicative of Mg-Li alloying and facilitated dissolution. *ACS Applied Materials & Interfaces* **2015**, *7*, 2494-2502.
39. Delsignore, M.; Farber, H.; Petrucci, S., Ionic conductivity and microwave dielectric relaxation of lithium hexafluoroarsenate (LiAsF₆) and lithium perchlorate (LiClO₄) in dimethyl carbonate. *The Journal of Physical Chemistry* **1985**, *89*, 4968-4973.
40. Petrucci, S.; Masiker, M. C.; Eyring, E. M., The possible presence of triple ions in electrolyte solutions of low dielectric permittivity. *Journal of Solution Chemistry* **2008**, *37*, 1031-1035.
41. Saar, D.; Brauner, J.; Farber, H.; Petrucci, S., Dielectric relaxation of some 1:1 electrolytes in tetrahydrofuran and diethyl carbonate. *The Journal of Physical Chemistry* **1978**, *82*, 1943-1947.
42. Buchner, R.; Chen, T.; Hefter, G., Complexity in "simple" electrolyte solutions: Ion pairing in MgSO₄(aq). *The Journal of Physical Chemistry B* **2004**, *108*, 2365-2375.

43. Borodin, O.; Douglas, R.; Smith, G.; Eyring, E. M.; Petrucci, S., Microwave dielectric relaxation, electrical conductance, and ultrasonic relaxation of LiPF₆ in poly(ethylene oxide) dimethyl ether-500. *The Journal of Physical Chemistry B* **2002**, *106*, 2140-2145.
44. Cavell, E. A. S.; Knight, P. C., Effect of concentration changes on permittivity of electrolyte solutions. *Zeitschrift für Physikalische Chemie* **1968**, *57*, 331.
45. Buchner, R.; Barthel, J., Kinetic processes in the liquid phase studied by high-frequency permittivity measurements. *J Mol Liq* **1995**, *63*, 55-75.
46. Pu, S. D.; Gong, C.; Gao, X.; Ning, Z.; Yang, S.; Marie, J.-J.; Liu, B.; House, R. A.; Hartley, G. O.; Luo, J., et al., Current-density-dependent electroplating in Ca electrolytes: From globules to dendrites. *ACS Energy Letters* **2020**, *5*, 2283-2290.

Table of Contents Graphic

